CHEMISTRY OF MATERIALS

ARTICLE

pubs.acs.org/cm

Effect of a Cobalt-Based Oxygen Evolution Catalyst on the Stability and the Selectivity of Photo-Oxidation Reactions of a WO_3 Photoanode

Jason A. Seabold and Kyoung-Shin Choi*

Department of Chemistry, Purdue University, West Lafayette, Indiana 47907, United States

Supporting Information

ABSTRACT: A bare WO_3 electrode and a WO_3 electrode coupled with a layer of Co−Pi oxygen evolution catalyst (OEC) were prepared to investigate the effect of Co−Pi OEC on the selectivity of photo-oxidation reactions and photostabilities of WO_3 photoanodes. WO_3 photoanodes have been reported to produce peroxo species as well as O_2 during photo-oxidation reactions, and the accumulation of peroxo species on the surface is known to cause a gradual loss of photoactivity of WO_3. The photocurrent to O_2 conversion efficiencies of the WO_3 and WO_3/Co−Pi OEC electrodes were obtained by simultaneously measuring the photocurrent and O_2 gas generated during illumination at 0.8 V vs Ag/AgCl. The result shows that the presence of OEC increases the photocurrent to O_2 conversion efficiency from approximately 61% to approximately 100%. The complete suppression of peroxo formation provided the WO_3/Co−Pi OEC photoelectrode with long-term photostability. The photocurrent−potential characteristics show that the presence of OEC effectively reduces the electron−hole recombination near the flat band potential region and shifts the onset potential of photocurrent by 0.17 V to the negative direction. However, when the applied potential became more positive than approximately 0.35 V vs Ag/AgCl, the WO_3/Co−Pi OEC electrode produced less initial photocurrent than the bare WO_3 electrode. Mott−Schottky plots reveal the presence of interface states at the WO_3/OEC junction that induce more electron−hole recombination when the Fermi level moves below these states. Regardless of the adverse effect on recombination present at 0.8 V vs Ag/AgCl, the WO_3/Co−Pi OEC achieved a more efficient and sustainable solar to O_2 conversion owing to the ability of Co−Pi OEC to significantly increase the photocurrent to O_2 conversion efficiency and prevent the photocurrent decay of the WO_3 electrode.

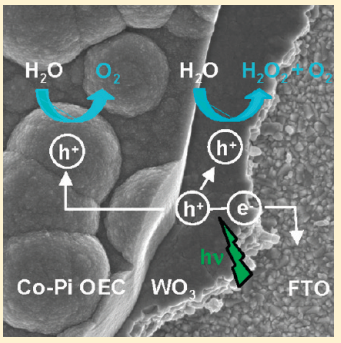

KEYWORDS: tungsten oxide (WO_3), photoanode, oxygen evolution catalyst, electrodeposition, solar energy conversion, photocurrent, photocorrosion

INTRODUCTION

WO_3, an n-type semiconductor with a bandgap of 2.7 eV, is a good photoanode for studying solar oxygen evolution in a water splitting photoelectrochemical cell.[1−8] It can utilize a portion of the visible spectrum to generate electron−hole pairs, and its valence band edge is located at approximately 3 eV versus NHE, providing enough overpotential to evolve oxygen.[9−11] WO_3 does not possess a conduction band capable of reducing H^+, but it can be coupled with a photocathode (i.e., p-type semiconductor) suited for solar H_2 production in the form of a photoelectrochemical diode or a tandem device to achieve solar water splitting.[4,5,12]

WO_3 is also predicted to be thermodynamically stable against anodic photocorrosion when used as a photoanode for a water splitting cell because its anodic decomposition potential is located 1.1 V more positive than the O_2 evolution potential.[13] However, it has been observed that WO_3 still suffers from a gradual loss of photoactivity during long-term use. Augustynski and co-workers reported that the loss of photoactivity of WO_3 is due to the formation and accumulation of peroxo species on the WO_3 surface.[3] This means O_2 production is not the only photo-oxidation reaction that occurs on the WO_3 surface, and a significant portion of the photon-generated holes are used to form peroxo species. Thermodynamically, oxidation of water to produce O_2 ($2H_2O \rightarrow 4H^+ + O_2 + 4e^-$, $E^o = 1.228$ V) is more feasible than the formation of peroxo species ($2H_2O \rightarrow 2H^+ + H_2O_2 + 2e^-$, $E^o = 1.776$ V).[14] However, due to the slow kinetics of the O_2 evolution reaction, the formation of peroxo species appears to become kinetically competitive with O_2 production. This understanding implies that if the kinetics for O_2 evolution are improved by placing a suitable O_2 evolution catalyst (OEC) on the WO_3 anode, it may be possible to suppress formation of peroxo species, which will increase the photostability of WO_3 while enhancing the efficiency of O_2 evolution.

In this study, we electrochemically prepared WO_3 and coupled it with a cobalt-based (Co−Pi) OEC, developed recently by Nocera et al., in order to study the effect of OEC on the photon-induced O_2 production and peroxide formation reactions of the

Received: July 13, 2010
Revised: December 9, 2010
Published: January 19, 2011

dx.doi.org/10.1021/cm1019469 | *Chem. Mater.* 2011, 23, 1105–1112

WO_3 electrode.[15−17] Typically, the performance of electrode-type photocatalysts (photoelectrodes) has been evaluated by measuring photocurrent, which provides information on how many electron−hole pairs are utilized for photodriven reactions. However, this measurement alone does not provide quantitative information on what portion of the photocurrents were used for desired reactions (e.g., H_2 or O_2 production for water splitting cells). Detecting H_2 or O_2 directly from colloid-type photocatalysts can provide a solar to H_2 or O_2 conversion efficiency, but this result alone cannot provide information as to what limits the efficiency (e.g., electron−hole pair generation/separation/transport vs presence of competing reactions). To quantitatively compare the selectivity of photo-oxidation reactions (i.e., O_2 production vs formation of peroxo species) occurring on the WO_3 electrode with and without OEC, we used a sealed photoelectrochemical cell equipped with an O_2 sensor and simultaneously measured both photocurrent and amount of O_2 produced. This measurement made it possible to estimate what percentage of photocurrent generated by WO_3 and WO_3/Co−Pi OEC anodes is actually involved with O_2 evolution (i.e., photocurrent to O_2 conversion efficiency).

The Co−Pi OEC has previously been coupled with ZnO and α-Fe_2O_3 photoanodes, and its ability to efficiently utilize photon-generated holes to enhance anodic photocurrent and/or O_2 evolution has been demonstrated.[18−20] In this study, we investigated the interactions of Co−Pi OEC with a WO_3 photoanode, in particular, whether it can selectively enhance the O_2 evolution reaction without increasing the kinetics of other competing photo-oxidation reactions. To the best of our knowledge, the issue of a Co−Pi OEC or any other OECs affecting the selectivity of water photo-oxidation by a photoanode has not been addressed in a quantitative manner. As a result of the known competing photo-oxidation reactions of the WO_3 electrode, this study provides a unique opportunity to investigate the role of the OEC on the selectivity of these reactions. We also examined the possibility of the Co−Pi OEC creating interface states at the WO_3/OEC junction that can affect electron−hole recombination in the WO_3 electrode. This becomes an important consideration when the OEC is paired with a photoanode to utilize photon-induced charge carriers for water splitting instead of being coupled with a conducting substrate to serve as a dark anode. This study will provide new insights on the various beneficial and adverse effects that can arise when the Co−Pi OEC is coupled with a photoanode for solar O_2 production.

EXPERIMENTAL SECTION

Materials. Cobalt chloride ($CoCl_2 \cdot 6H_2O$, 98%) was purchased from Sigma Aldrich. Hydrochloric acid (HCl, 36.5−38%) was purchased from JT Baker. Hydrogen peroxide (H_2O_2, 30%) and potassium hydroxide (KOH, pellets) were obtained from Mallinckrodt. Potassium phosphate monobasic (KH_2PO_4, ACS grade) and tungsten (W, <1 μm, 99.95%) were from Fisher and Alfa Aesar, respectively. All were used as purchased. Solutions were prepared using high purity water (Millipore Milli-Q purification system, resistivity > 18 MΩ).

Fluorine-doped tin oxide (FTO) was purchased from Hartford Glass, Incorporated. Platinum counter electrodes consisted of a glass slide with a 100 nm electron beam evaporated platinum layer on a 30 nm titanium adhesion layer.

Synthesis and Characterization. The WO_3 electrodes used in this study were electrodeposited following a previously reported procedure.[15] Solutions for electrodeposition were prepared by dissolving 2 g of W powder in 10 mL H_2O_2 (30%). Excess peroxide was decomposed using a small amount of platinum black with stirring. Then the solution volume was raised to 100 mL with water and the pH was adjusted to 1.35 with HCl. The final aqueous deposition solution contained 0.11 M tungsten as a peroxotungstate species and remained at room temperature throughout the deposition. A standard three-electrode cell was used, with an FTO working electrode, a Ag/AgCl (4 M KCl) reference, and a platinum counter electrode. All potential values reported in this study are against the Ag/AgCl (4 M KCl) reference electrode. Deposition of WO_3 films was carried out potentiostatically at −0.6 V for 6 min. A Princeton Applied Research VMP2 multichannel potentiostat was used for electrodeposition and all subsequent electrochemical studies. All freshly prepared WO_3 films were rinsed and then annealed at 500 °C for 1 h in air, with a 2 °C per minute ramping rate.

A Co−Pi OEC layer was then electrodeposited onto WO_3 electrodes using conditions reported by Nocera et al.[16] Films were deposited potentiostatically at 1.1 V from room temperature solutions containing 0.5 mM $CoCl_2$ and 0.1 M KH_2PO_4 at pH 7 using the same electrode arrangement as noted previously, except that the FTO working electrode in this case contained a layer of electrodeposited and annealed WO_3. The WO_3/Co−Pi OEC electrode investigated in this study contained an approximately 1.7 μm thick Co−Pi OEC layer which was deposited for six hours. After deposition, the WO_3/Co−Pi OEC electrodes were kept immersed in water before photoelectrochemical characterization to prevent drying and cracking of the OEC layer.

X-ray diffraction (XRD) was carried out using a Scintag X2 diffractometer (Cu Kα radiation) to confirm the purity and crystallinity of the prepared WO_3 electrode (Supporting Information, Figure S1). The morphologies of the WO_3 and Co−Pi OEC layers were examined by scanning electron microscopy using an FEI Nova NanoSEM 200 at an accelerating voltage of 5 kV. The SEM samples were first sputter coated with approximately 2 nm thick Pt.

Photoelectrochemical and Electrochemical Measurements. Photocurrent measurements utilized simulated solar illumination (AM 1.5G, 100 mW/cm^2) obtained by passing light from a 300 W xenon arc lamp through neutral density filters and an AM 1.5 filter into an optical fiber and calibrating the output to 100 mW/cm^2 (unless another intensity is noted). All samples were back-illuminated through the FTO glass to avoid absorption by the dark and thick catalyst layer. The illuminated area was 0.196 cm^2. All photocurrent and other electrochemical experiments were conducted in an argon-purged 0.1 M KH_2PO_4 electrolyte at pH 7, using the same three-electrode setup detailed above. Steady state photocurrent measurements used a bias voltage of 0.8 V. The linear sweep voltammogram (LSV) was scanned in the anodic direction at a scan rate of 10 mV/s. When illumination was used with an LSV, the chopping frequency was 1 Hz.

Capacitance was measured to obtain Mott−Schottky plots for WO_3 and WO_3/Co−Pi OEC electrodes using a Princeton Applied Research Potentiostat/Galvanostat model 263A connected to a Princeton Applied Research FRD100 frequency response detector. A sinusoidal perturbation of 10 mV was applied at frequencies of 1 kHz and 5 kHz. The three-electrode setup was used with a 0.1 M phosphate buffer at pH 7. All electrodes were masked with Teflon tape to expose the same geometrical area (0.4 cm^2) for measurement.

Oxygen Detection. Oxygen was detected quantitatively using an Ocean Optics fluorescence-based oxygen sensor (FOSPOR-R 1/16 in.). The electrochemical cell was a custom-built airtight two-compartment cell divided by a frit. One side held a Pt counter electrode, while the other side held the working electrode (WO_3 or WO_3/Co−Pi OEC) along with a Ag/AgCl reference electrode. Both sides were filled with 0.1 M KH_2PO_4, and the electrolyte and the headspace of the sealed cell were purged with argon. The electrolyte in the working compartment was 31.5 mL, and the headspace volume was 10.25 mL. The needle probe was inserted through a rubber septum and made continuous O_2 readings at 10 s intervals throughout the experiment. The probe was calibrated

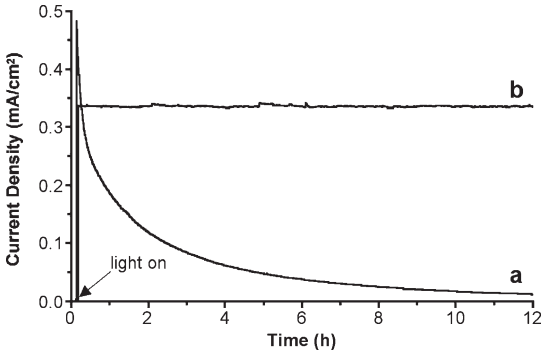

Figure 1. Photocurrent profiles of (a) a bare WO_3 electrode and (b) a WO_3/Co−Pi OEC electrode measured at 0.8 V vs Ag/AgCl in a 0.1 M phosphate buffer (pH 7) (illumination: AM 1.5G, 100 mW/cm^2).

using 2 points (argon, 0% O_2, and air, 20.9% O_2), with an error of 5% of the reading. The experiment began with 1 h of baseline O_2 measurement followed by 6 h of illumination using light passed through an AM 1.5 filter and adjusted to 400 mW/cm^2 (4 Suns) and 0.8 V applied bias. The use of an intense light (400 mW/cm^2) for the O_2 detection experiment was to ensure a higher signal-to-noise ratio and therefore more reliable data. There was a slight leak in the cell, seen by a slow rise of the baseline due to O_2 leaking in from the outside atmosphere (air contains 20.9% O_2), which was difficult to avoid completely due to the connection of three electrodes as well as the O_2 sensor to the cell. The leak rate was determined from the baseline measurement, and the data have been corrected for this leak rate (typically <0.09% total gas in the cell was exchanged per hour). The probe measures the O_2 content in the headspace and records as mole %. This was converted to micromoles after first adjustment for the O_2 dissolved in solution using Henry's Law. The charge passed during the experiment was also converted from coulombs to micromoles by dividing by 4F and multiplying by 10^6 (F = 96485 C/mol).

RESULTS AND DISCUSSION

The WO_3 electrodes used in this study were prepared by electrodeposition with an FTO substrate as the working electrode and were subsequently annealed at 500 °C for 1 h. The resulting WO_3 electrode was approximately 600 nm thick and had a flat and featureless surface. Photocurrent of a bare WO_3 electrode measured using simulated solar illumination and 0.8 V bias in a 0.1 M phosphate buffer at pH 7 is shown in Figure 1a. The photocurrent began to decline immediately, losing 63% of its initial value within the first hour. The photocurrent decay continued over 12 h, eventually resulting in a complete loss of photoactivity.

An SEM image of the WO_3 electrode after 2 h of photocurrent measurement shows a significant change in the film morphology when compared with a fresh WO_3 electrode (Figure 2a,b). The grains appear to shrink in size, and the electrode becomes porous, implying that the electrode is losing material via a dissolution process. This causes the gradual structural disintegration of the electrode and the reduction of photoactivity.

The severe structural disintegration shown in Figure 2b was observed only at the site of illumination, indicating that it is associated with a photoelectrochemical process. An electrode exposed to identical conditions for 2 h but kept in the dark (Figure 2c) shows that only subtle dissolution along the grain boundaries occurs when compared with the fresh WO_3 electrode, suggesting that chemical dissolution of WO_3 is not as severe as photodissolution. However, an SEM image after extended soaking

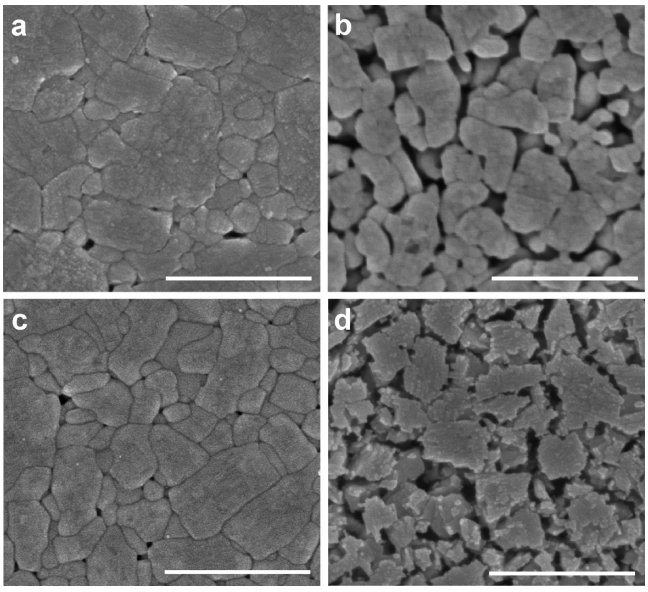

Figure 2. SEM images of (a) fresh, (b) 2 h illuminated, (c) 2 h soaked (in the dark), and (d) 24 h soaked (in the dark) WO_3 electrodes. All except (a) were in 0.1 M KH_2PO_4 pH 7 buffer (scale bar, 500 nm).

(24 h) under the same electrolyte in the dark shows that chemical dissolution also becomes a problem after long-term exposure of WO_3 to the neutral electrolyte used in this study (Figure 2d).

The photocorrosion process observed during the photocurrent measurement indicates that oxygen evolution via water oxidation is not the sole photo-oxidation reaction occurring at the bare WO_3 electrode. An obvious alternate photo-oxidation reaction, which may result in the loss of photoactivity or photodissolution of WO_3, is the formation of peroxo species at the WO_3 surface.[3] Surface bound peroxo species can be formed by oxidation of surface hydroxyl groups of the WO_3 electrode or by oxidation of water/hydroxide to hydroxyl radicals or peroxides which then adsorb on the WO_3 surface to form tungsten peroxo species.[21] Formation of surface bound peroxo species has been observed during illumination of various n-type semiconductors, including TiO_2 and $Ca_2Nb_3O_{10}$ as well as WO_3.[3,22−24] In each of these cases, it resulted in a loss of photoactivity of the semiconductor.

To confirm that the photoinstability observed with our WO_3 system is also due to the generation of surface bound peroxo species, we performed LSVs to detect the electrochemical reduction of these species. The LSV of a 2 h illuminated WO_3 electrode shows the emergence of a peak at −0.3 V that is not present in the LSV of the fresh WO_3 electrode (Figure 3a,b). This reduction peak matches well with the literature description of surface peroxo reduction on TiO_2, which confirms the generation of surface peroxo species on our WO_3 electrodes.[23,25] It should be noted that a fresh electrolyte purged with argon gas was used for each measurement and electrodes were rinsed between each step of the experiment to ensure that any new peaks which appeared were due to an electrode-bound species and not any species generated free within the electrolyte.

Previous studies on surface bound peroxo species of WO_3 and $Ca_2Nb_3O_{10}$ showed that these species can be eliminated from the oxide surface via thermal oxidation, and the heat procedure fully restores the lost photoactivity.[3,24] When we repeated an LSV after heating the WO_3 electrode for one hour at 500 °C, peroxo species were no longer present at the surface (Figure 3c).

dx.doi.org/10.1021/cm1019469 |*Chem. Mater.* 2011, 23, 1105–1112

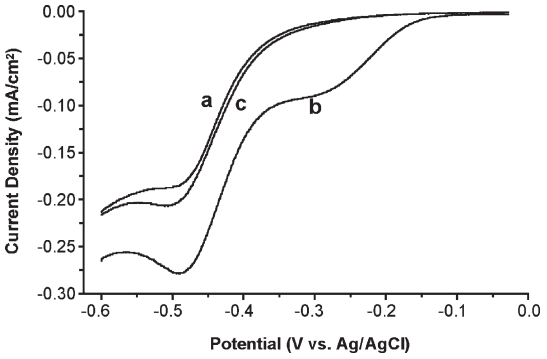

Figure 3. LSVs of (a) a bare WO_3 electrode and the same electrode subjected to (b) 2 h of illumination and then (c) heat treated at 500 °C. Each LSV was performed in a fresh 0.1 M KH_2PO_4 pH 7 buffer using a scan rate of 10 mV/s.

However, the original photocurrent performance was never fully restored, only reaching approximately 75% photocurrent recovery (Supporting Information, Figure S2). This is because the formation of tungsten peroxo species on the WO_3 surface in our case resulted not only in surface deactivation but also in successive dissolution of the newly formed tungsten peroxo species. While the photoactivity loss via surface deactivation can be regained by thermal removal of the peroxo species, the loss via dissolution is permanent. Previous studies that observed a full recovery of photoactivity after a thermal treatment most likely dealt with metal peroxo species that are less soluble than the tungsten peroxo species and/or used an electrolyte pH which could minimize the dissolution of the metal peroxo species. Since the solubility of tungsten peroxo species decreases with decreasing pH, the use of an acidic electrolyte may minimize the dissolution of the generated tungsten peroxo species. However, the formation of surface deactivating tungsten peroxo species occurs regardless of the electrolyte pH if the electrolyte contains no other hole accepting species that can be oxidized more readily than water.[3]

In this study we chose a neutral phosphate electrolyte because our intention was to investigate the possibility of using Co−Pi OEC, which is not stable in an acidic medium, to prevent the formation of peroxo species and therefore the photoactivity loss of WO_3. Identifying conditions to operate a WO_3 anode in a neutral medium may also be beneficial if it is coupled with a p-type semiconductor which is not stable in an acidic medium to construct a photoelectrochemical diode.

To investigate the effect of OEC on the stability and selectivity of photo-oxidation reactions of WO_3, Co−Pi OEC was electrochemically deposited on the WO_3 electrodes following previously reported conditions.[16,17] Figure 4 shows cross-sectional and top-view SEM images exposing the layers of a WO_3/Co−Pi OEC electrode. We intentionally electrodeposited a thick OEC layer (>1.5 μm) to use it as a physical barrier to minimize direct contact between WO_3 and the electrolyte, which may alleviate the aforementioned chemical dissolution problem. The Co−Pi OEC layer may not serve as a completely impermeable protecting layer, and water may still reach the surface of WO_3 through the layer. However, we postulated that due to slow or limited diffusion in the water within the Co−Pi OEC layer, initial chemical dissolution of WO_3 would result in the saturation of WO_4^{2-} species at the WO_3/water interface within the catalyst layer, preventing further dissolution of WO_3.

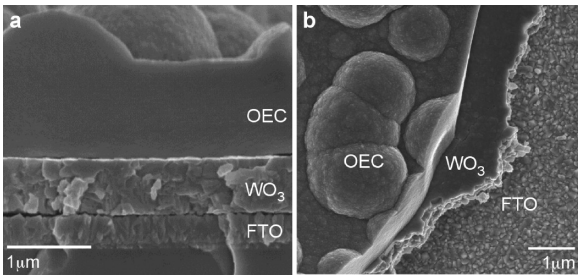

Figure 4. (a) Cross-sectional and (b) top-view SEM images revealing the layers of a WO_3/Co−Pi OEC electrode deposited on an FTO substrate.

The photocurrent profile of WO_3/Co−Pi OEC is displayed in Figure 1b. In contrast to bare WO_3, the photocurrent remains stable over long periods of time. We tested up to 12 h and observed no sign of instability. This indicates that the presence of Co−Pi OEC effectively suppresses the formation of surface bound peroxo species, preventing photochemical deactivation of the WO_3, while protecting it from chemical dissolution. With this data alone, however, it is not clear whether the presence of Co−Pi OEC truly inhibits the formation of peroxo species or merely prevents the formation of tungsten peroxo species by generating peroxide species not at the WO_3/electrolyte interface but at the OEC/electrolyte interface. The illuminated area of the WO_3/Co−Pi OEC sample formed bubbles steadily while the bare WO_3 electrode did not show significant bubbling, indicating that indeed a greater number of photon-generated holes are used for O_2 evolution when the Co−Pi OEC is present. However, a more quantitative analysis is necessary to compare the selectivity of photo-oxidation for O_2 evolution in the presence and absence of Co−Pi OEC (i.e., photocurrent to O_2 conversion efficiency).

To obtain photocurrent to O_2 conversion efficiencies, we measured the O_2 gas produced by the bare WO_3 and the WO_3/Co−Pi OEC electrodes using a fluorescence-based O_2 sensor while also recording the photocurrent at 0.8 V. Then the amount of O_2, which was calculated from the generated photocurrent by assuming 100% Faradaic efficiency, was compared with the actual amount of detected O_2. The result shows that the bare WO_3 electrode utilized only 61% of separated holes for O_2 evolution (Figure 5a). The anodic current produced by the remaining 39% of the holes is attributed to the formation of the peroxo species which is responsible for the gradual decay of photoactivity seen for the bare WO_3 electrode. On the other hand, the WO_3/Co−Pi OEC electrode utilized 100% of its photocurrent to produce O_2 (Figure 5b) and completely suppressed the formation of peroxo species, which agrees well with the long-term stability observed for the WO_3/Co−Pi OEC electrode. This result demonstrates that Co-based OEC selectively improves the kinetics of the O_2 evolution reaction such that the formation of peroxo species can no longer compete with O_2 evolution.

LSVs of the WO_3 and WO_3/Co−Pi OEC electrodes in the dark were obtained to compare the catalytic nature of these electrodes for electrochemical O_2 evolution. Figure 6a shows that the presence of a Co−Pi OEC layer shifts the onset potential for O_2 evolution to the positive direction by approximately 500 mV. (The shoulder directly before O_2 onset by the WO_3/Co−Pi OEC electrode is due to the oxidation of Co^{2+} ions in the Co−Pi OEC.)[16] The potentials applied to the WO_3 and WO_3/Co−Pi OEC electrodes to achieve an anodic current of 3.0 mA/cm^2 are 1.85 and 1.09 V, respectively, more than a 750 mV difference.

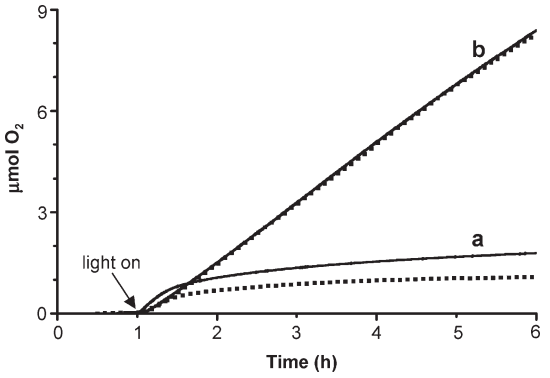

Figure 5. O_2 detected by a fluorescence based sensor (---) and O_2 calculated from charge passed (—) during illumination of (a) a bare WO_3 electrode and (b) a WO_3/Co−Pi OEC electrode (light intensity: 400 mW/cm^2, applied bias: 0.8 V vs Ag/AgCl).

This significant improvement in O_2 evolution capability from the WO_3 to the WO_3/Co−Pi OEC electrode explains why the product composition (O_2 vs H_2O_2) of the water photo-oxidation reaction on the WO_3 electrode varied significantly when the Co−Pi OEC layer was added.

It may be necessary to point out the fundamental difference between electrochemical and photoelectrochemical O_2 and H_2O_2 evolution. For electrochemical oxidation, the overpotential available to drive a reaction is determined by applied potential. In Figure 6a, when O_2 evolution begins, there is no competition with H_2O_2 production because the H_2O_2 reaction cannot occur until a more positive potential is reached. However, for photo-oxidation the overpotential available to drive any reaction is determined, not by the applied potential, but by the position of the valence band edge. The photon-generated holes in the valence band of WO_3 have enough potential to achieve both O_2 evolution and H_2O_2 production. Therefore, competition between these two reactions can occur independent of the applied potential under illumination and their kinetics can significantly affect the yield of the products.

The effect of Co−Pi OEC was also studied by measuring current−potential characteristics with a chopped light, which simultaneously shows dark current and photocurrent in a single sweep (Figure 6b). This measurement shows that the onset potential for photocurrent of the bare WO_3 is −0.03 V vs Ag/AgCl. This value is shifted to the positive direction by 0.25 V from the flat band potential (V_{fb}) of the bare WO_3 electrode, −0.28 V vs Ag/AgCl, which was determined by Mott−Schottky plots (Figure 6c). A positive shift of the photocurrent onset from the flat band potential is commonly observed for n-type semiconductors and is caused by slow kinetics and/or surface recombination that reduce the photocurrent to zero before the bands become completely flat.

When the same measurement was carried out with a WO_3/Co−Pi OEC electrode, photocurrent near the flat band potential of the WO_3 electrode was significantly enhanced and the photocurrent onset potential was shifted to −0.20 V. This clearly indicates that the presence of the Co−Pi OEC layer effectively reduces recombination near the flat band potential region. Photocurrent stability and the photocurrent to O_2 conversion efficiencies of the WO_3 and WO_3/Co−Pi OEC electrodes obtained in this low band bending region (i.e., at E = 0.2 V vs Ag/AgCl) can be found in Supporting Information (Figure S3). The WO_3/Co−Pi OEC electrode shows an enhanced photocurrent stability, and

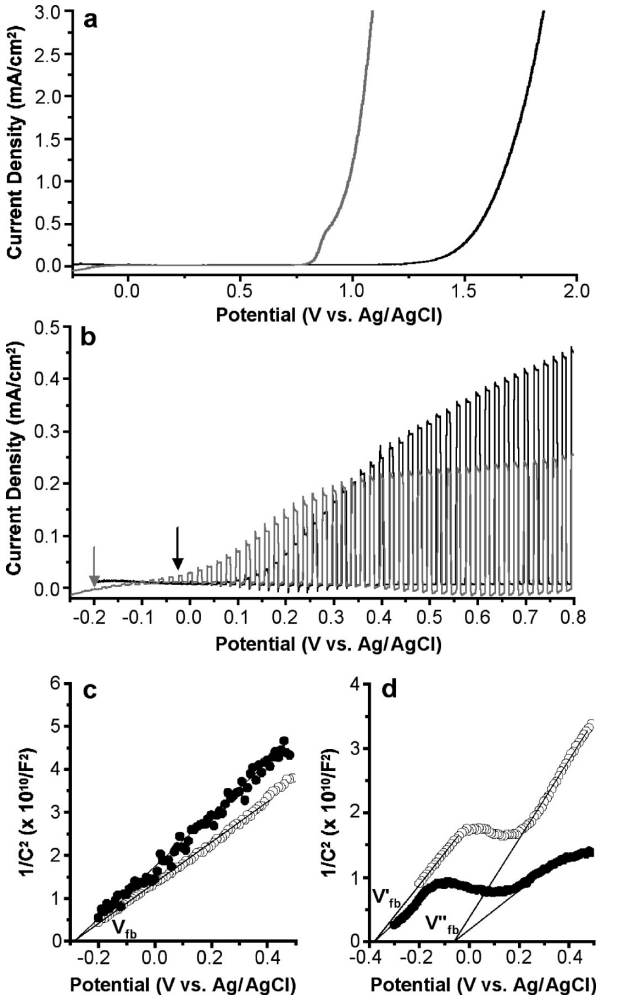

Figure 6. LSVs of (a) a WO_3 electrode (black) and a WO_3/Co−Pi OEC electrode (gray) in the dark and (b) the same electrodes under chopped illumination (AM 1.5G, 100 mW/cm^2) measured in 0.1 M KH_2PO_4 buffer (pH 7) with a scan rate of 10 mV/s. Arrows in (b) indicate the onset potential of photocurrent. The slight cathodic dark current observed in (b) for the WO_3/Co−Pi OEC electrode between 0.4 and 0.8 V is due to the electrochemical reduction of Co^{3+} in the Co−Pi OEC layer to Co^{2+}. Mott−Schottky plots of (c) WO_3 and (d) WO_3/Co−Pi OEC electrodes at 1 kHz (○) and 5 kHz (●). The flat band potential, V_{fb}, was consistent regardless of the changes in frequency.

the photocurrent to O_2 conversion efficiencies of the WO_3 and WO_3/Co−Pi OEC electrodes were approximately 60% and approximately 100%, respectively, which are essentially identical to those obtained at 0.8 V.

When the applied bias becomes more positive, however, the difference between photocurrent generated from the bare WO_3 and that from WO_3/Co−Pi OEC is gradually reduced, and above approximately 0.35 V the photocurrent of the bare WO_3 electrode actually exceeds that of the WO_3/Co−Pi OEC electrode. We have already confirmed with the results shown in Figures 1 and 5 that the photocurrent generated in the bare WO_3 electrode is not an exclusive result of O_2 production and it quickly decays. However, the fact that the WO_3 electrode initially generates a higher photocurrent in this potential range does imply that less recombination occurs in the bare electrode compared with the WO_3/Co−Pi OEC electrode. This phenomenon is also observed in Figure 1 where the initial photocurrent

dx.doi.org/10.1021/cm1019469 |Chem. Mater. 2011, 23, 1105–1112

Scheme 1. Schematic Band Diagrams of (a) a Bare WO_3 Electrode and (b) a WO_3/Co−Pi OEC Electrode Showing the Changes in the Flat Band Potential and Band Bending Depending on the Applied Bias[a]

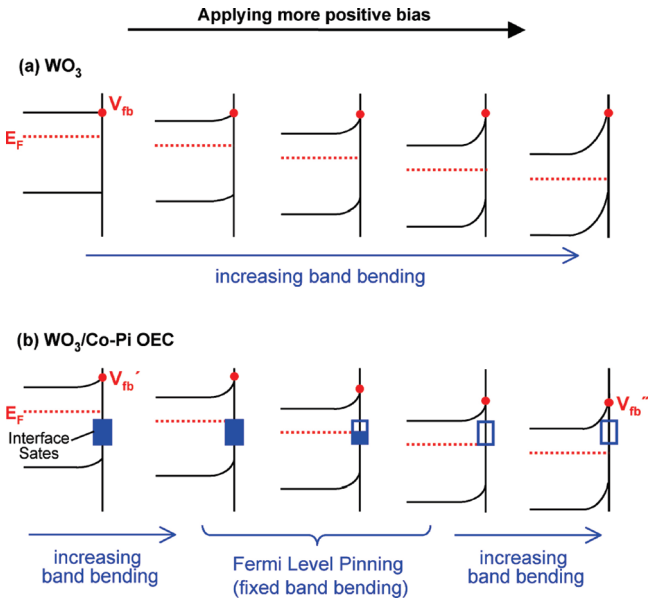

[a] E_F = Fermi level, V_{fb} = flat band potential.

generated by the bare WO_3 is higher than that of the WO_3/Co−Pi OEC electrode. These observations indicate that while the presence of Co−Pi OEC reduces recombination near the flat band potential, it actually increases recombination when the applied bias becomes more positive.

The most plausible explanation for the phenomenon observed in Figure 6b is the presence of interfacial states in the WO_3/Co−Pi OEC electrode that are generated by the Co ions present at the WO_3/Co−Pi OEC junction. Judging from the fact that the Co−Pi OEC reduces recombination near the flat band potential, these states are probably located a few hundred millivolts more positive than the flat band potential of the WO_3, and they increase electron−hole recombination as the applied potential moves beyond the level of these states in the positive direction.

The presence of these interface states was experimentally confirmed by a Mott−Schottky plot of the WO_3/Co−Pi OEC electrode (Figure 6d). This plot shows a region where the capacitance is independent of voltage. This feature, which is absent in the Mott−Schottky plot of the bare WO_3 photoelectrode, is a clear indication of a high density of deep, monoenergetic interface states located at the WO_3/Co−Pi OEC junction.[26] When the applied potential (and therefore the Fermi level) is within the interface state band so that the interface states are partially occupied (Scheme 1, center), the Fermi energy is pinned and the band bending will be independent of the applied potential.[26,27] When the applied potential is more negative than these interfacial states so that the states are fully occupied, the excess negative charges present at the interface shift the flat band potential to the negative direction (V_{fb}' in Figure 6d).[26] As a result, the WO_3/Co−Pi OEC electrode will generate more band bending than the WO_3 electrode at any potential within this range (Scheme 1, left), thus decreasing electron−hole recombination. On the other hand, when the applied potential is more positive than these interfacial states and the interface states are

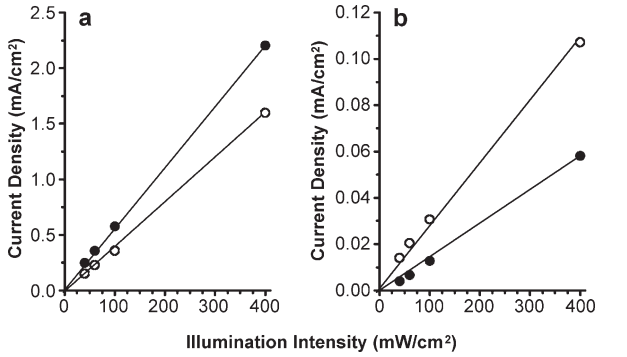

Figure 7. Light intensity dependent photocurrent of a bare WO_3 electrode (●) and a WO_3/Co−Pi OEC electrode (○) measured (a) at 0.8 V and (b) 0.1 V vs Ag/AgCl.

completely emptied, the excess positive charges accumulated at these states shift the flat band potential to the positive direction (V_{fb}'' in Figure 6d).[26] This results in a lower degree of band bending in the WO_3/Co−Pi OEC electrode than in the WO_3 electrode at potentials within this range (Scheme 1, right), thus generating less photocurrent. The effect of the WO_3/Co−Pi OEC interface states on electron−hole recombination can be beneficial or adverse depending on the potential applied. This explanation agrees well with the observed potential−photocurrent characteristics in Figure 6b.

The capacitance−potential characteristics of the Co−Pi OEC layer deposited on an FTO substrate can be found in Supporting Information (Figure S4). The capacitance of the Co−Pi OEC layer bears no similarity to the capacitance of the WO_3/Co−Pi OEC electrode or the capacitance difference between the WO_3 and WO_3/Co−Pi OEC electrodes. This suggests that the difference in the Mott−Schottky plots shown in Figure 6c,d is due to the modification of the WO_3/electrolyte interface caused by the interaction between the WO_3 surface and the Co−Pi OEC layer.

We also considered the possibility that the lower photocurrent of the WO_3/Co−Pi OEC electrode when $E > 0.35$ V is due to a kinetic limitation of O_2 evolution at the Co−Pi OEC/electrolyte interface. In the more positive bias region, a higher band bending is created and more holes are transferred from the WO_3 photoanode to the Co−Pi OEC layer. If the hole transfer rate from the Co−Pi OEC to water molecules (i.e., O_2 evolution rate) is limited, holes will accumulate in the Co−Pi OEC layer, which may cause more electron−hole recombination in the WO_3/Co−Pi OEC electrode than in the bare WO_3 electrode. We tested this possibility by measuring photocurrent of the WO_3/Co−Pi OEC electrode under various light intensities at 0.8 V (Figure 7a). The photocurrents show a linear dependence on the light intensity. In particular, the fact that the photocurrent generated by the WO_3/Co−Pi OEC electrode linearly increased from 0.4 to 1.6 mA/cm^2 when the light intensity was increased from 100 mW/cm^2 to 400 mW/cm^2 confirmed that the photocurrent of the WO_3/Co−Pi OEC electrode in the positive bias region of Figure 6b was not limited by the O_2 evolution kinetics of the OEC. The light intensity-dependent photocurrent of the bare WO_3 electrode is also shown in Figure 7a for comparison. It also exhibits a linear dependence, but its slope is steeper than that of the WO_3/Co−Pi OEC electrode because of the adverse effect of the interface states present in the WO_3/Co−Pi OEC electrode at 0.8 V. The same experiment was carried out at 0.1 V where the adverse effect of the interface states is not present in the WO_3/Co−Pi OEC

dx.doi.org/10.1021/cm1019469 |*Chem. Mater.* 2011, 23, 1105–1112

electrode (Figure 7b). Under this condition, the photocurrents of both the WO_3 and WO_3/Co−Pi OEC electrodes also showed a linear dependence on the light intensity but the WO_3/Co−Pi OEC electrode generated more photocurrent, as expected. The photocurrents used to make these plots were recorded at each light intensity five seconds after illumination was initiated. This enabled the determination of the photocurrent value after the initial transient photocurrent was stabilized, while avoiding the long-term photodecay effect of the WO_3 electrode.

Our study demonstrated various ways that the Co−Pi OEC can affect the performance of a WO_3 photoanode. Some of these effects are of no concern when OEC is used as an electrocatalyst on a conductive dark anode for electrolysis of water. However, they can become critical issues when the OEC is coupled with a semiconductor electrode that utilizes photon-induced charge carriers for solar water splitting. For the WO_3/Co−Pi OEC system studied here, the recombination effect caused by the interface states in the region $E > 0.35$ V was not significant compared to the improvement made by the OEC in preventing the photocurrent decay and enhancing the photocurrent to O_2 conversion efficiency. As a result, the WO_3/Co−Pi OEC electrode produced O_2 much more efficiently than the bare WO_3 electrode even when it was operated at 0.8 V where the recombination effect was the most pronounced (Figure 5). Whether the presence of OEC on a photoanode will create interface states of any significance (either beneficial or adverse) depends greatly on the type of semiconductor, the details of the photoanode/OEC junction structures, the interfacial energetics/kinetics, and the operating conditions of the cell (e.g., relative positions of the interface states, flat band potential, band edge positions, applied potential). Analyzing and understanding all of the advantages and drawbacks created by placing an OEC on a photoanode and gaining the ability to manipulate interfacial structures to maximize synergistic interactions while minimizing adverse effects will be critical in the production of photoanode/OEC systems that can achieve high solar to O_2 conversion efficiencies.

CONCLUSIONS

We have studied the photo-oxidation reactions and photostability of electrochemically prepared WO_3 and WO_3/Co−Pi OEC photoanodes in a neutral 0.1 M phosphate buffer solution. When a bare WO_3 photoanode was used, a significant portion of the photogenerated holes (ca. 39%) were used to form peroxo species which accumulated on the WO_3 surface resulting in a gradual loss of photoactivity. As a result of the pH of the electrolyte, the formation of tungsten peroxo species also resulted in dissolution and structural disintegration of the WO_3 electrode. When a thick Co−Pi OEC layer (>1.5 μm) was deposited on the WO_3 electrode, however, all photon-generated holes were used for O_2 production, indicating that the Co−Pi OEC can selectively enhance the O_2 evolution reaction. The complete suppression of the peroxide species not only increased O_2 production but also provided WO_3 with long-term photostability. The micrometer thick OEC layer also prohibited the chemical dissolution of the WO_3 electrode in the neutral medium. The photocurrent−potential characteristics showed that the Co−Pi OEC layer increased photocurrent near the flat band potential by reducing electron−hole recombination, which shifted the photocurrent onset potential by 170 mV to the negative direction. However, as the applied bias became more positive (>0.35 V), the WO_3/Co−Pi OEC electrode began to produce less photocurrent than the WO_3 electrode, and this photocurrent difference became more pronounced as the applied potential was further increased. This phenomenon is due to Co ions at the planar WO_3/Co−Pi OEC junction which create interface states that shift the flat band potential to the negative direction when occupied and to the positive direction when emptied, as confirmed by Mott−Schottky plots. As a result, the WO_3/Co−Pi OEC electrode suffers less from electron−hole recombination than the WO_3 electrode when the Fermi level is above the interfacial states and more when the Fermi level is below the interfacial states. This study revealed the various effects that the Co−Pi OEC can have on a WO_3 photoanode for solar O_2 production, which can guide us to better design of photoanode/OEC systems. The WO_3 electrode used in this study was not optimized to enhance photon absorption, charge transport properties, or surface area. We expect that with the use of more efficient WO_3 anodes and proper interfacial optimization to control the interface states, a more efficient WO_3/Co−Pi OEC system can be built.

ASSOCIATED CONTENT

Supporting Information. XRD of WO_3 electrode, photocurrent plot of WO_3 electrode showing partial recovery after thermal removal of peroxo species, photocurrent and O_2 detection of WO_3 and WO_3/Co−Pi OEC electrodes at 0.2 V vs Ag/AgCl, and capacitance−potential plots of WO_3 and WO_3/Co−Pi OEC electrodes as well as a Co−Pi OEC layer on FTO (PDF). This material is available free of charge via the Internet at http://pubs.acs.org.

AUTHOR INFORMATION

Corresponding Author

*E-mail: kchoi1@purdue.edu. Tel: 1-765-494-0049. Fax: 1-765-494-0239.

ACKNOWLEDGMENT

This work was financially supported by the Center for Chemical Innovation of the National Science Foundation (Grant CHE-0802907) and made use of the Life Science Microscopy Facility at Purdue University.

REFERENCES

(1) Santato, C.; Odziemkowski, M.; Ulmann, M.; Augustynski, J. *J. Am. Chem. Soc.* **2001**, *123*, 10639–10649.
(2) Santato, C.; Ulmann, M.; Augustynski, J. *Adv. Mater.* **2001**, *13*, 511–514.
(3) Augustynski, J.; Solarska, R.; Hagemann, H.; Santato, C. *Proc. SPIE* **2006**, *6340*, U140–U148.
(4) Wang, H. L.; Deutsch, T; Turner, J. *J. Electrochem. Soc.* **2008**, *155*, F91–F96.
(5) Miller, E. L.; Marsen, B.; Paluselli, D.; Rocheleau, R. *Electrochem. Solid-State Lett.* **2005**, *8*, A247–A249 (tandem).
(6) Cole, B.; Marsen, B.; Miller, E.; Yan, Y.; To, B.; Jones, K.; Al-Jassim, M. *J. Phys. Chem. C* **2008**, *112*, 5213–5220.
(7) Berger, S.; Tsuchiya, H.; Ghicov, A.; Schmuki, P. *Appl. Phys. Lett.* **2006**, *88*, 203119-1–203119-3.
(8) de Tacconi, N. R.; Chenthamarakshan, C. R.; Yogeeswaran, G.; Watcharenwong, A.; de Zoysa, R. S.; Basit, N. A.; Rajeshwar, K. *J. Phys. Chem. B* **2006**, *110*, 25347–25355.
(9) Xu, Y.; Schoonen, M. A. A. *Am. Mineral.* **2000**, *85*, 543–556.

(10) Bak, T.; Nowotny, J.; Rekas, M.; Sorrell, C. C. *Int. J. Hydrogen Energy* **2002**, *27*, 991–1022.
(11) van de Krol, R.; Liang, Y. Q.; Schoonman, J. *J. Mater. Chem.* **2008**, *18*, 2311–2320.
(12) Nozik, A. J. *Annu. Rev. Phys. Chem.* **1978**, *29*, 189–222.
(13) Gerischer, J. In *Solar energy conversion*; Seraphin, B. O., Ed.; Springer: Berlin, 1979; pp 115−172.
(14) Pourbaix, M. *Atlas of Electrochemical Equilibria in Aqueous Solutions*, 2nd English ed.; National Association of Corrosion Engineers: Houston, 1974.
(15) Meulenkamp, E. A. *J. Electrochem. Soc.* **1997**, *144*, 1664–1671.
(16) Kanan, M. W.; Nocera, D. G. *Science* **2008**, *321*, 1072–1075.
(17) Surendranath, Y.; Dinca, M.; Nocera, D. G. *J. Am. Chem. Soc.* **2009**, *131*, 2615–2620.
(18) Steinmiller, E. M. P.; Choi, K. S. *Proc. Natl. Acad. Sci. U.S.A.* **2009**, *106*, 20633–20636.
(19) Zhong, D. K.; Sun, J. W.; Inumaru, H.; Gamelin, D. R. *J. Am. Chem. Soc.* **2009**, *131*, 6086–6087.
(20) Zhong, D. K.; Gamelin, D. R. *J. Am. Chem. Soc.* **2010**, *12*, 4202–4207.
(21) Oosawa, Y.; Grätzel, M. *J. Chem. Soc., Chem. Commun.* **1984**, *24*, 1629–1630.
(22) Yesodharan, E.; Yesodharan, S.; Gratzel, M. *Sol. Energy Mater.* **1984**, *10*, 287–302.
(23) Ulmann, M.; Detacconi, N. R.; Augustynski, J. *J. Phys. Chem.* **1986**, *90*, 6523–6530.
(24) Compton, O. C.; Osterloh, F. E. *J. Phys. Chem. C* **2009**, *113*, 479–485.
(25) Augustynski, J. *Electrochim. Acta* **1993**, *38*, 43–46.
(26) Morrison, S. R. *Electrochemistry at Semiconductor and Oxidized Metal Electrodes*; Plenum Press: New York, 1980; pp 153−188.
(27) Bard, A. J.; Bocarsly, A. B.; Fan, F.-R. F.; Walton, E. G.; Wrighton, M. S. *J. Am. Chem. Soc.* **1980**, *102*, 3671–3677.